Lab on a Chip

Bubble-particle dynamics in multiphase flow of capillary foams in porous micromodel

Journal:	*Lab on a Chip*
Manuscript ID	LC-ART-05-2023-000419.R1
Article Type:	Paper
Date Submitted by the Author:	15-Aug-2023
Complete List of Authors:	Okesanjo, Omotola; Georgia Institute of Technology, Chemical and Biomolecular Engineering Aubry, Guillaume; School of Chemical & Biomolecular Engineering, Georgia Institute of Technology, Behrens, Sven; Georgia Institute of Technology, School of Chemical & Biomolecular Engineering; Exponent Inc, Polymer science and Materials chemistry Lu, Hang; Georgia Tech, Chemical and Biomolecular Engineering Meredith, J.; Georgia Institute of Technology, School of Chemical and Biomolecular Engineering

ARTICLE

Bubble-particle dynamics in multiphase flow of capillary foams in a porous micromodel

Received 00th January 20xx,
Accepted 00th January 20xx

DOI: 10.1039/x0xx00000x

Omotola Okesanjo,‡[a] Guillaume Aubry,‡[a], Sven Behrens*[ab], Hang Lu*[a] and J. Carson Meredith*[a]

Surfactant-free capillary foams (CFs) are known to be remarkably tolerant to oil, and possess unique stability and flow properties. These properties result from the presence of oil-and-particle-coated bubbles that are interconnected by a dense particle-oil capillary network. In this work, we present a study of the dynamics of capillary foams flowing through a porous micromodel. We determine that despite the presence of oil-particle networks, CFs can flow through a microporous environment and that above a threshold flowrate, >80% of foam pumped through the micromodel can be recovered. In addition, we highlight the absence of steady state in CF flow and identify the underlying phenomena including the increasing apparent viscosity, reconfigurable flow paths, and intermittent clogging of the micromodel from oil-particle composite and bubbles trapped in pores. We also characterize bubble dynamics and show that CFs surprisingly exhibit the same bubble generation and destruction mechanisms as classical foams despite the absence of surfactants. Our observations suggest that the porous medium plays a key role in generating uniformly sized bubbles and that capillary foams in a microporous environment tend to reconfigure their flow paths in a manner that may provide opportunities for increased sweep efficiency in enhanced oil recovery.

Keywords: Capillary foams, Porous media, Microfluidics, Bubbles, Multiphase flow

1. Introduction

Foams are the focus of intense research because their remarkable properties find applications in a wide range of fields, such as pharmaceutics, cosmetics, firefighting, froth floatation and oil recovery.[1-2] For example, foams have the potential to mitigate low sweep efficiency caused by gravity override and viscous fingering in gas-injection enhanced oil recovery (EOR).[3] The high apparent viscosity and ability to reduce gas mobility by trapping the gas within liquid barriers make foams potentially better displacing fluids for EOR than their single-phase counterparts.[3-5] Therefore, further studies of foam behavior in microporous environments are essential to improving oil recovery strategies.

Many studies have been devoted to probe the pore-scale displacement dynamics of foams for EOR and other transport applications in porous media.[6-8] These studies focus on foams stabilized by surfactant or surfactant-nanoparticle blends and were conducted in various microenvironments, such as sandpack, glass, polydimethylsiloxane (PDMS) templated and 3D-printed micromodels.[5, 9-13] However, some limitations remain from the intrinsic properties of these foams. Only a limited number of surfactant foams (SFs) show adequate stability to oil, high temperature and saline reservoir conditions.[14] Nanoparticle stabilized foams have been found to perform better than surfactant foams due to their ability to reduce and delay the entrance and spreading of oil droplets that destroy foam films.[13] Further investigation of foams with improved performance is necessary to bring new insights and strategies in transport applications in porous media.

Foams of yet another type, the more recently discovered capillary foams (CFs),[15] are very oil tolerant,[16] but their flow through porous media has not yet been studied. CFs are stabilized by the synergistic action of particles and a small amount of an immiscible liquid (oil) that mediates capillary interactions.[17] The gas bubbles in CFs are coated by a composite layer of oil and particles, and they are interconnected via a network of particles bridged by the oil (**Fig. 1a**).[15, 18] The composition and architecture of CFs offer excellent foam stability over days, even in the presence of oil, and exhibit strong elasticity under stress.[19-20] The fundamental flow properties of CFs were previously probed in rheology and foam flow experiments that revealed a non-zero yield stress and high viscosities comparable to those of high-quality surfactant foams.[19] Foam flow studies suggest that the plug flow profile of CFs could enable uniform fluid displacement in transport applications and that the network strength and stability of an existing foam can be increased through additional shearing.[16] CF tunability and stability under stress and in the presence of oil may be advantageous to enhanced oil recovery.[19, 21-22]

[a] School of Chemical and Biomolecular Engineering, Georgia Institute of Technology, Atlanta, Georgia 30332, USA.
Email: hang.lu@chbe.gatech.edu; carson.meredith@chbe.gatech.edu
[b] Polymer Science & Materials Chemistry, Exponent Inc., Atlanta, Georgia 30326, USA.
‡ These authors contributed equally
Electronic Supplementary Information (ESI) available: [details of any supplementary information available should be included here]. See DOI: 10.1039/x0xx00000x

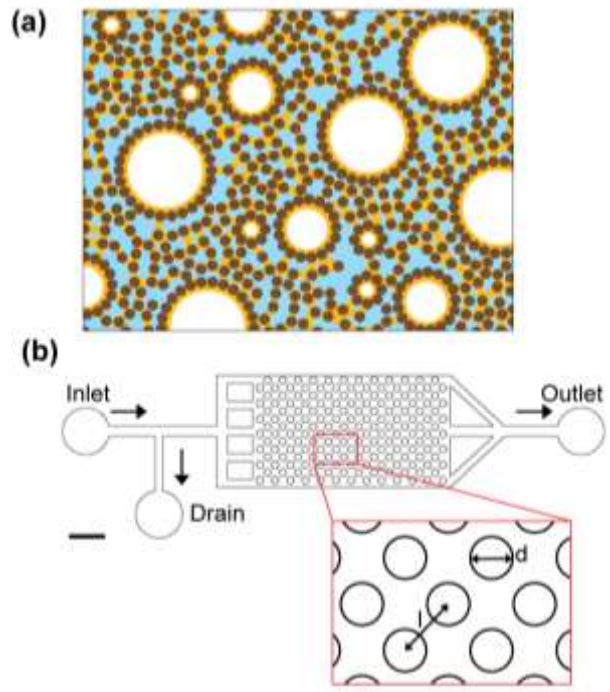

Fig. 1 Schematic of capillary foam and micromodel of porous environment. (a) Capillary foam (CF) structure composed of a network of oil-coated bubbles and oil-bridged particles. (b) PDMS-based micromodel used to study CF behavior in a microenvironment. The foam propagates through the micropillar array (d = 200 µm, l = 300 µm). Scalebar: 1 mm.

Although the dynamics of foams and their ability to displace oil from porous media has been studied extensively,[23-25] to our knowledge, the pore-scale dynamics of a quaternary-phase colloidal system like CFs has not been reported. No study has ever been carried out on the properties of CFs flowing through a porous environment, and to our knowledge, there are only few existing studies that detail the pore scale behavior of low-quality foams or bubbly liquids as exemplified by colloidal gas aphrons.[26] The structural differences in CFs compared to SFs, *i.e.*, the presence of two types of fluid interfaces and a network of particles, are likely to increase the complexity of the dynamics and displacement characteristics of foams at the pore scale. Thus, it is important to understand the benefits and practicality of applying CFs through micromodel studies like those conducted on SFs. Fundamental micromodel studies of CFs will answer questions on how the particle network and observed bubble rigidity in CFs influence clogging, foam propagation, and bubble breakup frequency.

In this article, we study the dynamics of capillary foams flowing through a PDMS-templated micromodel by using high speed video microscopy to probe the mechanics of bubbles and particles at the pore length scale. We discuss capillary foam mobility and stability within the porous medium. Lastly, we highlight and explain the observed bubble and particle interactions, pore clogging remediation mechanisms, and bubble dynamics.

2. Materials and Methods

2.1 Reagents

Amorphous fumed silica particles modified with dichlorodimethylsilane and containing 50% residual SiOH on the surface were provided by Wacker-Chemie AG (Germany). Particle size and zeta potential were determined by dynamic and electrophoretic light scattering using a Malvern Zetasizer Nano ZS90. The hydrodynamic radius of the silica particles in 5 mM NaCl solution at pH 4.9 is 403 nm. Trimethylolpropane trimethacrylate (TMPTMA) was obtained from Sigma-Aldrich. Deionized water (DI water) was used as the primary aqueous phase. Foams were prepared using a rotor-stator homogenizer (IKA Ultra-Turrax T10, rotor diameter of 6.1 mm, stator diameter 8 mm).

2.2 Capillary foam preparation

Silica particles were first dispersed in methanol. The particle solution was centrifuged, and the methanol supernatant was removed. The particle sediment was rinsed by re-suspending the particles in DI-water, sonicating the solution to properly disperse the particles and finally centrifuging the solution. The silica particles were rinsed at least five times to ensure that methanol is effectively removed from the suspension.

Silica particles were suspended at 1.5 wt. % in DI-water containing 5 mM NaCl salt. TMPTMA (oil-phase) was added to silica suspension at 1 wt. %. This UV-curable oil was used in the earlier studies of capillary foams, where confocal microscopy and scanning electron microscopy were used to probe the foam architecture and understand the location of the oil.[15, 18, 21] Although other oil-particles systems have been explored as well, systems with TMPTMA as the oil phase are the most studied example of CFs and were thus selected for this study. Silica particles used in this study are hydrophilic ($\theta_{awp} \sim 30° \pm 10°$) and have previously been shown to stabilize oil-in-water emulsions with equal volumes of TMPTMA and water.[18] We note that these particles are preferentially wetted by the aqueous phase and connect the silica particles used here in a capillary state network.[27] We have previously studied the effect of particle wettability on the oil-particle network bridging in capillary foams and summarize here that when the continuous fluid (water) preferentially wets the particles, capillary bridges are formed between the particle and the oil, however, when the secondary fluid (oil) preferentially wets the particles, pendular bridges are formed. We have also previously shown that the strength of the capillary bridges in CFs are influenced by the amount of oil in the foam.[18] In this work, we have used 1wt. % of TMPTMA oil because this system has been found to provide a good balance of strong bridges without hindering foam mobility during flow in a tube.[16]

Capillary foams were prepared by mechanically frothing the oil-water-particle mixture in a 20 ml Vial or in the barrel of a 10 ml BD syringe (for foam flow experiments) with the IKA Ultra-Turrax at 30,000 rpm for 2 minutes. During frothing, the position of the mixer head is alternated between the surface and the bottom of the mixture at 20-30secs intervals. At the onset of frothing, the mixer is placed at the surface of the

mixture to introduce air into the system. Subsequently, the mixer is submerged into the mixture to allow for high shear mixing of the particle and fluids. The oil-particle composite forms the basis of the CFs. During frothing, particles are first connected by oil bridges. Following the formation of the oil-particle network, particle-assisted spreading of oil around the air-water interface stabilizes gas bubbles and the oil-particle network helps to entrap the oil-coated bubbles thus completing foam formation.

2.3 Design of the microporous environment

To mimic a soil environment, we created a 2D artificial porous medium (**Fig. 1b**) composed of a periodic micro-structured array. Circular pillars of 200 µm in diameter were organized in a centered rectangular lattice to obtain a pore size of 100 µm (**Table 1**). This 2D porous environment (height ~ 80 µm) enabled optical access of the entire micromodel and, with the use of dyes, enabled quantitative analysis via image processing.

Table 1 Characterization of the microporous environment shown in Fig. 1. and for a chamber height of 80 μm.

Post Diameter (μm)	Pore Size (μm)	Porosity (%)	Permeability (Darcy)	Pore Volume (nl)	Wettability
200	100	65	462	4.7	Hydrophobic

2.4 Fabrication of the microfluidic device

Device fabrication was performed using conventional soft lithography techniques.[28] The master was fabricated by spin coating two SU8-photoresist layers on a silicon wafer. The first layer (15 μm, SU8-2015) was used as an adhesion layer. The second layer (80 μm, SU8-2050) was used for molding the microfluidic channels via optical lithography. After development, the master was coated overnight with an anti-adhesive (tridecafluoro-1,1,2,2-tetrahydrooctyl-1-trichlorosilane). A mixture of 10:1 PDMS/crosslinker was poured on top of the master and left to cure for 2 h in a 90 °C oven. Afterwards, PDMS slabs were cut off for each individual device and access wells were punched using biopsy punchers (1 mm diameter puncher for the inlet and 5 mm diameter puncher for the outlet). Finally, each PDMS block was bonded to a glass slide via plasma treatment.

2.5 Foam flow experiments

Capillary foams prepared in 10 ml BD syringe barrel and were allowed to drain and settle for 20 min. The water at the bottom of the foam was first removed and then the CFs were pumped through polytetrafluoroethylene (PTFE) tubing (ID: 0.034”; OD: 0.52”) or silicone tubing (ID: 0.031”; OD: 0.094”) into a PDMS microfluidic device using a New Era (model 1010) syringe pump as shown in **Fig. S1**. The effluent from the device was collected downstream in a 20 ml vial. Multiple devices were used for each experiment. The devices were degassed and filled with water prior introducing the foam except otherwise stated.

2.6 Imaging and pressure monitoring

Capillary foams flowing through the porous environment were imaged using optical light microscopy on an upright stereo microscope (Leica, Model MDG36, 3x magnification). A Phantom V7 high-speed camera (4000 fps) was attached to the microscope to record foam behavior at different conditions.

The pressure upstream and downstream of the micromodel was monitored via 206 KPa (30 psi) serial sensors (Honeywell, model: 24PCDFG6G). The sensors were connected to home-made board circuits including two-operational amplifiers (Texas Instrument, INA126) and various resistors to adjust the gain. The read-out was performed via an Arduino system (chipKIT uC32 Arduino – programmable PIC32 Microcontroller board, Digilent) and a home-made LabVIEW interface.

2.7 Image processing

Microscopy images were processed and colored using ImageJ and Adobe Photoshop software. Videos were analyzed using home-made MATLAB programs. Briefly, bubble information (number, size, position) was extracted from binary images obtained via simple thresholding. Clogged areas were determined by thresholding the variance of pixel intensity over a 10-frame sliding window at 30 fps.

3. Results

3.1 Foam stability

To assess the suitability of capillary foams for transport through porous media, we determined CF recovery after flow through the PDMS micromodel. Given the intricate foam architecture and network connectivity in CFs (**Fig. 1a**), the stability and mobility of CFs in a porous environment is not obvious *a priori*; the expectation is that the particle network may clog the pores and prevent foam flow or that phase separation will occur due to breakdown of the particle network as the foam is forced through the medium. However, we show here that capillary foams maintain relative foam stability and mobility over a range of flow rates ($\dot{v}$) when pumped through the micromodel. In **Fig. 2a**, the image comparison between an unpumped CF (left) and a CF recovered from the micromodel (right) highlights the high recovery of foam after flowing through the micromodel and demonstrates that, despite the network strength and connectivity, CFs can flow through and retain their structures after being pumped through a microporous environment.

CF recovery through the porous micromodel is dependent on the flow rate. Image comparison in **Fig. 2a** shows that the recovered foam head when CFs are pumped at $\dot{v} = 0.1$ ml/min is smaller than the foam head recovered when $\dot{v} = 0.8$ ml/min. We quantified the percentage of foam volume recovered relative to the foam volume pumped into the micromodel for different flow rates in **Fig. 2b**. Although CFs can progress through the pore spaces, more CF is recovered at the high and intermediate flow rates relative to the low flow rate (0.1 ml/min).[16] At low flow, the stress imposed hastens CF aging and leads to CF loss over time due to phase separation as shown

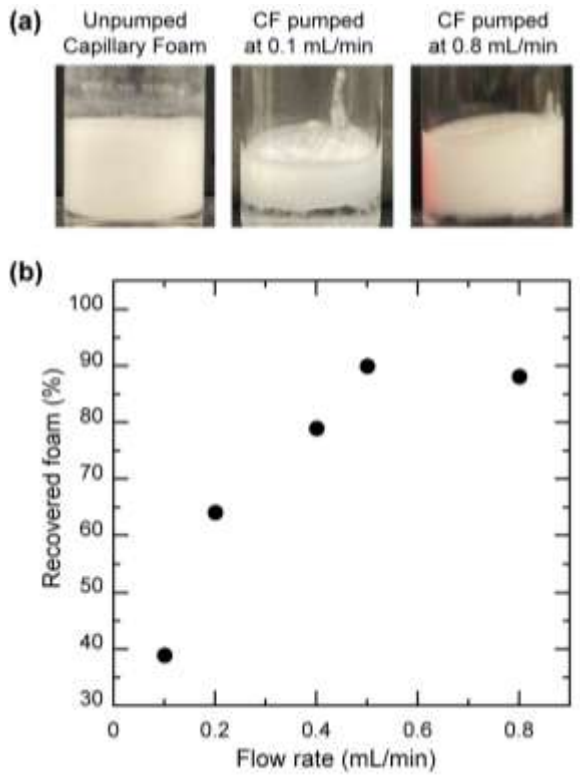

Fig. 2 Impact of flow rate on CF stability as CF is pumped through porous micromodel. (a) Comparison of images of an unpumped capillary foam versus a capillary foam collected after the foam flew through micromodel for different flow rates. (b) Percentage of capillary foam recovered as a function of flow rate.

by the segregated regions of gas slugs, water, and foams in the tube (see **Fig. S2**). In addition, clogging, which occurs more at lower flow rates, also amplifies the loss of recoverable CF by facilitating flow of water through the foam matrix in a process reminiscent of drainage.

The observations in **Fig 2** are well aligned with results of our previous study on stability of CFs flowing through a millimeter size tube where we observed that the CF volume recovered after foam flow, in a tube, increases with flow rate.[16] That work also showed that the stability of CFs is controlled by drainage within the first hour of foam preparation and subsequently controlled by coarsening in later hours. Drainage in CFs can result in foam volume changes of up to 20% within the first hour, however no significant volume changes are measured afterwards. We note that foam volume changes were not observed during coarsening. Drainage and coarsening can be significantly limited by strengthening the particle network via increasing the particle volume fraction within the foam. However, the particle network strength needs to be moderated so as not to inhibit CF flow. The recovery of CFs from the porous environment underscores the robustness of the foam stabilization mechanism in CFs. We will devote the rest of this article to explaining the characteristic phenomena of CF flow through porous environment.

3.2 Foam flow behavior characterized by the absence of steady state

We observed 3 stages during CF flow through the micromodel, regardless of the flow rate: I) an initial stage that consists of particle aggregates in suspension flowing through the pores, II) a middle stage where bubbles and particle aggregates co-flow or alternate through the pores, III) a final stage chiefly consisting of gas slugs moving through the pores. **Fig. 3** shows images of the micromodel during CF flow at each stage; videos of foam flow during each stage can be found in the supporting file (see **Vid. S1**). The 3 stages identified are due to both the foam composition and experimental set-up. The CFs pumped through the micromodel in this work have low gas volume fractions (~ 30-40 vol. %) compared to typical surfactant foams (> 80 vol. %) and are inherently wet foams. When the syringe piston is pushed downward, as shown in the experimental setup in **Fig. S1**, the water and particle suspension at the outlet of the syringe are first displaced and move through the pore spaces in the micromodel. The foam head, containing small and medium size bubbles, in the middle of the syringe follows afterwards and the top portion of the CF containing gas slugs, closest to the piston, enters the micromodel last.

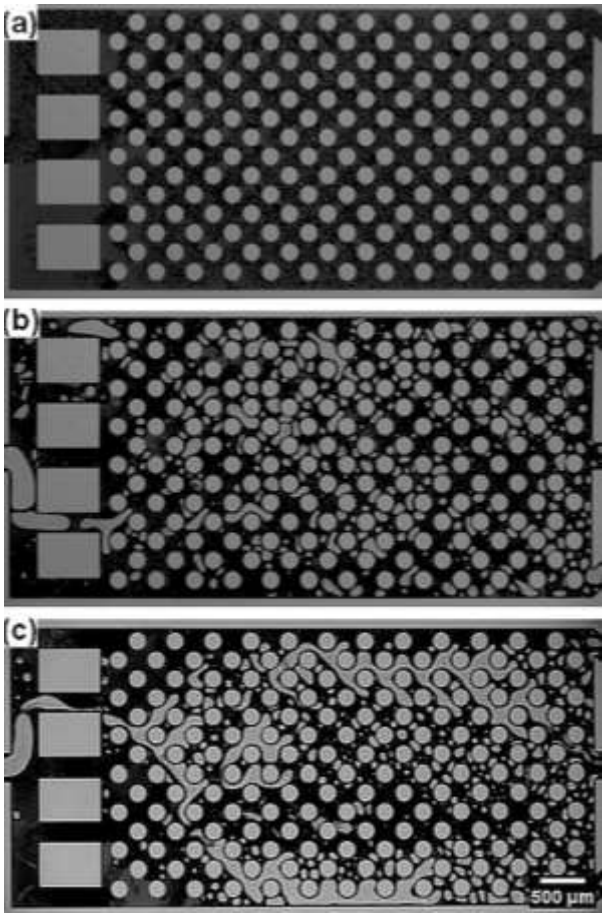

Fig. 3 Optical micrographs showing different stages in capillary foam flow (a) initial particle aggregate flow (stage I), (b) co-flow of particles and bubbles (stage II) and (c) gas slug invasion of pores (stage III).

To further characterize the CF flow and differentiated behavior with the flow rate, we monitored the pressure differential (ΔP) across the micromodel. **Fig. 4** shows the pressure differential versus dimensionless time ($\tau = t/t_f$) measured when CFs are pumped through the micromodel at different flow rates (where t_f is the total duration of the experiment corresponding to the time required to pump the prepared CF volume through the micromodel at each flow rate). The three regimes (I, II, and III) of ΔP versus t shown in **Fig. 4** correspond to the 3 different stages highlighted in **Fig. 3** above. At all flow rates explored, the pressure drop across the micromodel increases with time. The gaps in the recordings correspond to points where we had to readjust the gain of the amplifier circuit of the pressure sensor to expand the range of the sensor. The pressure differential for the high and intermediate flow rates steadily increases throughout the experiment and eventually exceeds the capacity of the pressure sensor (~220 KPa). In contrast, the pressure increase at the lowest flow rate is not as pronounced as that of other flow rates.

At the onset of CF flow, i.e., stage I, suspended particles and small particle aggregates flow easily through the porous environment and maintain a steady $\Delta P \leq 10$ kPa. This occurs because particles are reasonably well dispersed and do not hinder foam flow by clogging the pores. As foam flow continues, the particle aggregates entering the pores become larger and some eventually get entrapped, likely because of the affinity of the pore walls for the oil that bridges the particles. The flow of particle aggregates in suspension occurs for a small portion of the entire foam flow experiment, as bubbles start to invade the pore shortly after the larger particle aggregates pass through the micromodel.

In stage II, $0.2 \leq \tau \leq 0.65$, the pressure starts to rise within moments of entry of the first set of bubbles and dense particle aggregates. Co-flow of bubbles and particle aggregates change the flow dynamics within the pores as more pores entrap both bubbles and particles and reduce the number of flow paths available to the foam within the porous environment. The increase in ΔP with dimensionless time ($\tau \sim 0.2$) results from the initial entrapment of bubbles and particle aggregates within the pores, thus limiting the available pathway for foam flow. The initial pressure increase enables the mobilization of CFs through available paths while leaving dead zones (portions without flow) in the micromodel. When foam flow is continuous, ΔP remains nearly constant as bubbles and particle aggregates move through 1-2 available paths; however, this typically lasts only for tens of seconds. Because the foam flow pathways within the micromodel occasionally change as existing paths clog and others are freed up, the overall foam sweep of the micromodel volume is high with <20% permanent dead zones.

In stage III, when $\tau \geq 0.65$, sharp increases in ΔP are observed as foam flow approaches the top region of the CF in the syringe because gas slugs and fewer suspended particles or aggregates flow through the pores. CF flow in this stage becomes more discontinuous because of compressibility and mobilization of gas slugs. The high ΔP in this regime causes foam mobilization through the pores; the pressure significantly

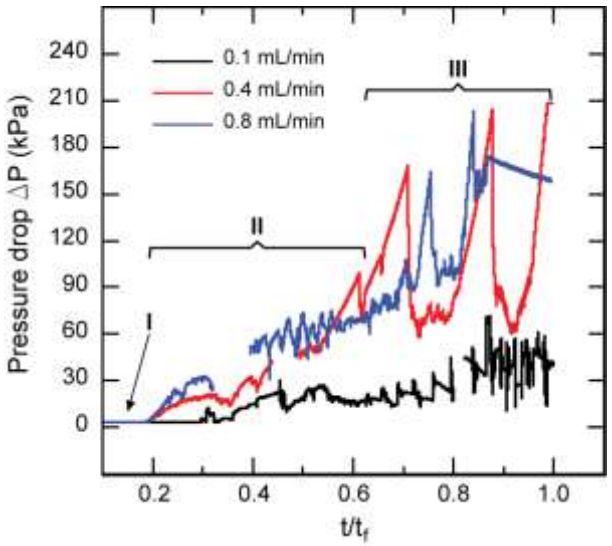

Fig. 4 Pressure drop versus dimensionless time (τ) required to mobilize capillary foams through the micromodel at different pumping speeds during particle aggregate flow (stage I), co-flow of particles and bubbles (stage II) and flow of large gas slugs (stage III).

decreases when bursts of foam flow occur but increases again as foam flow slows. CF flow in stage III is more discontinuous than in stage I and II as more clogging occurs because the foam is drier and more compressible due to gas slugs.

The observed fluctuations and overall increase in ΔP show that CF flow through the porous medium does not approach steady state during the foam flow experiments. One potential reason for the fluctuations in ΔP during CF flow through the porous medium could be the multiphasic nature of CF (water, particle aggregates and bubbles). Although the particle network and bubbles in CFs are connected by oil bridges, some of the connections are likely broken to form a simpler suspension of bubbles and particle aggregates in water during flow.[29] At low flow rates, we observe that phase separation of the foam into plugs of water, gas, and particle suspension can occur in the piping before the foam approaches the micromodel. The fluctuations in ΔP are obviously also related to the level of pore clogging. We will explore, in the next sections, the influence of foam viscosity and how varying levels of clogging with time change the driving force required to mobilize the CFs through the pores.

3.3 Impact of foam viscosity and clogging on flow resistance and remediation mechanisms

To understand pressure increases during CF flow, we studied the two major contributors to the flow resistance within the system: the foam viscosity and channel clogging. We quantify the flow resistance due to foam viscosity by estimating the apparent viscosity (η) of the capillary foam in the micromodel through Darcy's law:

$$\dot{v} = \frac{kA}{\eta L}\Delta P \qquad (1)$$

where $\dot{v}$ is the volumetric flow rate, k is the permeability, A is the cross-sectional area, L is the length of the flow path, and ΔP is the pressure drop. Considering only the flow segments where ΔP is relatively stable and with the simplifying assumptions that i) the CF flow through the micromodel is homogenous, and ii) the absolute permeability of CFs can be approximated as that of a single phase via the scaling argument of the Kozeny-Carman equation,[30-32] the apparent viscosity of CFs pumped at the intermediate and high flow rates was found to range between 45 – 170 cP. This viscosity is significantly higher than the viscosity of water and comparable to that of crude oils.[33-35] At the lowest flow rate (0.1 ml/min), the notion of apparent viscosity loses meaning given the unsteady nature of flow and the lack of a consistent velocity. The estimated high viscosity suggests that CFs may prove as effective as high-quality surfactant foams in inducing the high flow resistance in porous environments needed to restrict gas mobility and improve sweep efficiency during oil recovery.[6, 25, 36]

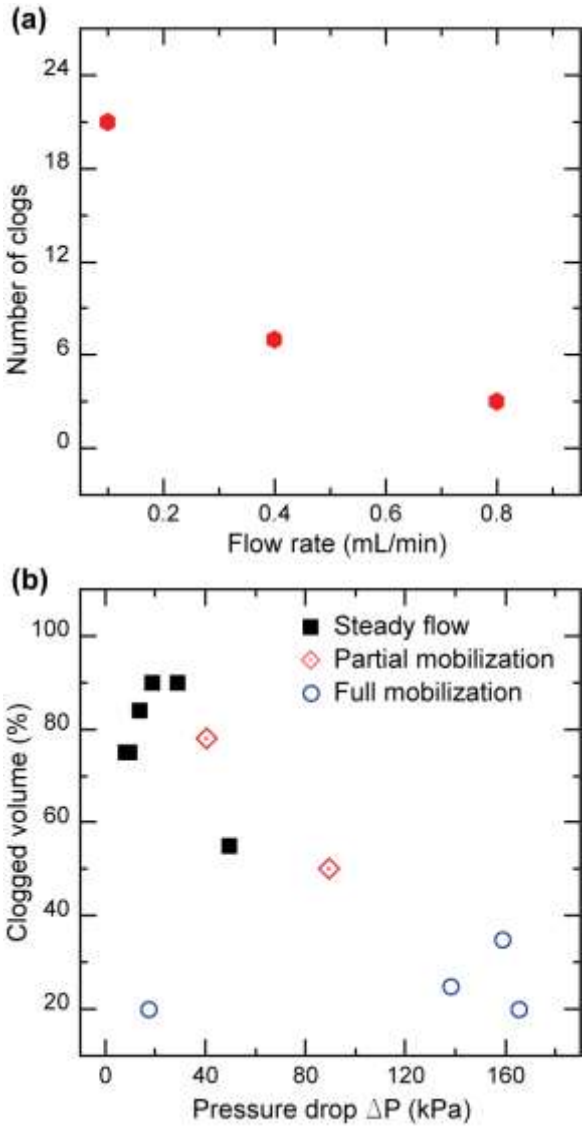

Fig. 5 Impact of flow rate and pressure on clogging during CF flow through the micromodel. (a) Number of full/ complete clogging events with flow rates. (b) Pressure required to mobilize CFs and percent of micromodel clogged at different pressures.

The second main source of variation in pressure drop is pore clogging. Particles and bubbles trapped within the micromodel increase the overall flow resistance and lead to spikes in ΔP. We observed that particle aggregates and bubbles can clog the pore space either partially or completely when they are unable to move through the pore constrictions (See **Vid. S2**). Partial clogging is said to occur when the foam flows through only few channels because bubbles and particles are trapped in some of the pores while full (or complete) clogging when foam flow is obstructed across the entire micromodel. Regardless of the imposed flow rate, we observed that the preponderant regime is the partial clogging for most of the CF flow duration. On the other hand, the occurrence of temporary complete clogging varies with flow rate and the duration of clogging is highly variable. **Fig. 5a**, shows the number of complete clogging events observed at different flow rates when ~7 ml of CF is pumped through the micromodel. Complete clogging decreases with increasing flow rate, which suggests that a higher rate of foam propagation may preclude clogging in CF flow through porous environments. The number of complete clogs correlates with the spikes and fluctuations in ΔP seen at different flow rates in **Fig. 3**; we observe more fluctuations in ΔP at the lowest flow rate than at the intermediate and high flow rates.

Clogs occur when the local pressure is unable to overcome the resistance of capillary forces from oil-coated bubbles and oil bridges in particle aggregates. Foam flow in a porous environment is influenced by viscous and capillary forces, both of which are functions of the degree of capillary bridging in the foam, the applied pressure from the pump and the interfacial tensions in the flowing foam. When capillary forces dominate viscous forces, as is the case when flow velocity is low, foam flow can become clogged. The low and slow build-up of pressure at low flow rates (**Fig. 3**) suggests that the capillary forces resist the applied pressure and thus only a small portion of the CF is mobilized at a given time interval when the foam yields to the applied pressure. At higher flow rates, on the other hand, the higher driving force helps to mobilize CFs through the device with fewer clogs, because capillary forces are easily overcome. Furthermore, as pressure builds in system, the bubbles in CFs coarsen and contribute to the capillary pressure that further resists the foam flow.

The number of clogs (complete clogging) in the micromodel not only influences the free flow of CFs through the micromodel but also prevents adequate reformation/ strengthening of the foam. Previous studies on CF flow show that foam flow at high shear results in foam preservation and can also lead to the formation of stronger networks in CFs.[16] Foam flow at low shear however results in an increase in drainage, coarsening and eventual phase separation within CFs. When clogging occurs, the upstream force required to overcome the clog increases and drives phase separation of fluids within the CFs. We can therefore infer that there is a 1-to-1 correlation between the number of complete clogs and the acceleration of drainage and coarsening in CFs that leads to reduced foam stability and foam recovery during CF flow in the micromodel.

Clogging during CF flow is temporary and is resolved through multiple mechanisms such as pressurization, erosion, and path switching explained below. We observe that pressurization at the inlet of the micromodel remediates clogging by forcing the CFs through the micromodel pores at high pressures; the inlet pressure drops significantly when foam flow continues, and the clog has been cleared (See **Vid. S2**). In erosion, a current of water sweeps away particles and bubbles trapped in the pores of the micromodel and opens new channels for foam flow (See **Vid. S3**). Erosion can occur through the process of viscous fingering, where water flows through the porous CF matrix that is higher in viscosity. Finally, path switching occurs when new flow paths open as the existing paths close (See **Vid. S4**). Because the foam flow takes the path of least resistance, path switches take place when the clogging of another path in the micromodel is weak. One or more of these processes can take place at the same time; for example, path switching can occur during erosion. Partial mobilization, where one or two paths open after a complete clog, can occur via all the above-mentioned processes; we note, however, that erosion and pressurization typically lead to full mobilization that alleviates clogs in multiple pores in the micromodel.

The clogged volume of the micromodel during CF flow correlates with the pressure drop. In **Fig. 5b**, we plot the clogged fraction of the micromodel as a function of the measured pressure drop when CFs flow through the pores. The plot shows that at low pressures ($\Delta P \leq 34.4$ KPa), except for the blue circle at ($\Delta P = 17.2$ KPa), at least 70% of the pore volume is clogged. At intermediate pressures, $34 \leq \Delta P \leq 124$ KPa, roughly half of the pores are clogged, and above 138 KPa, 35% or less of the pores are clogged. The low pressures and high clogged volume points (black squares) in **Fig. 5b** correspond to flow through only 1 or 2 channels in the micromodel. The higher-pressure data points, with lower clogged volumes, capture situations of pressurization and clogging remediation where mobilization occurs in multiple channels within the micromodel.

3.4 Bubble dynamics/Behavior of flowing bubbles

While pore scale mechanisms of bubble formation and destruction are well characterized for surfactant foams,[6] CF bubble dynamics at the pore scale has not previously been explored. Nor is it intuitive that the behavior of CF bubbles should closely resemble bubble behavior in classical foams: the added rigidity imparted on the CF bubbles by their particle-stabilized oil-coat and especially the absence of fast-diffusing surfactants capable of quickly covering any freshly created interface might be expected to prevent CFs from mimicking the self-regenerating behavior of surfactant foams traveling through porous media. Yet we surprisingly observed that CF bubbles flowing through pores interact with one another and with constrictions in the way familiar from surfactant foams, and that they exhibit well-known bubble generation and destruction mechanisms. We show, in **Fig. 6a-c**, lamella division, pinch off and snap off bubble division and generation

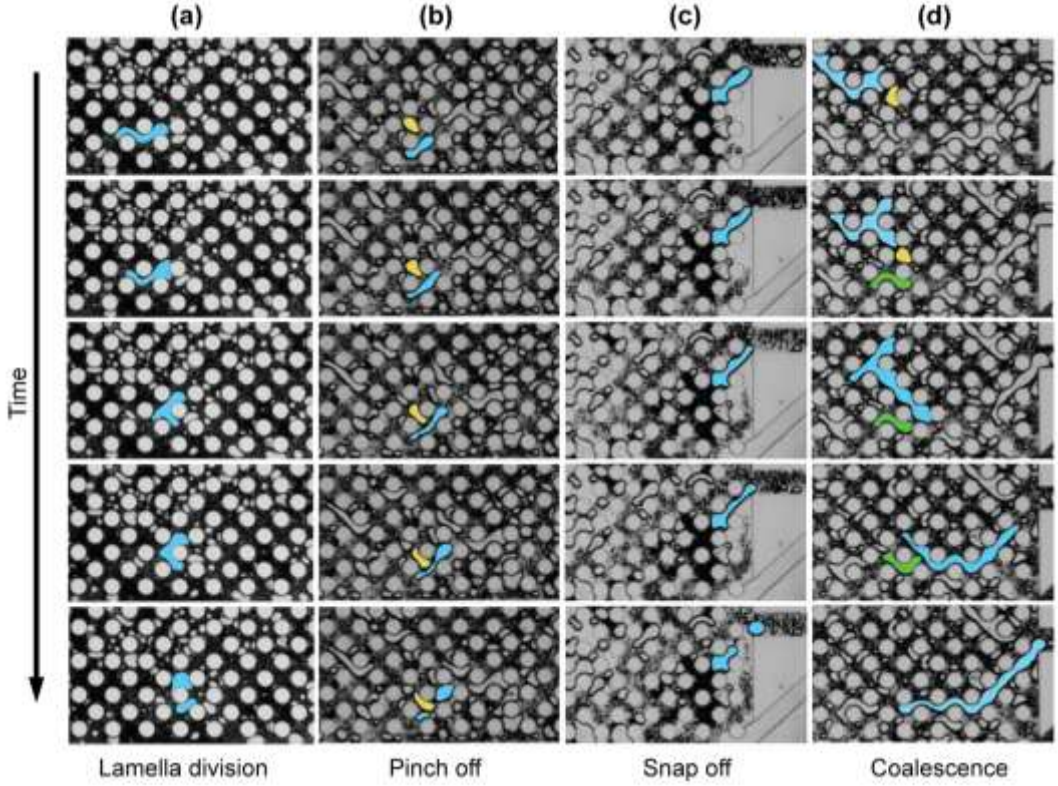

Fig. 6 Optical micrographs showing bubble division and generation mechanisms in CF flowing through microporous environment: (a) lamella division, (b) pinch off, (c) snap off and (d) coalescence. Bubbles are fake colored for illustration purpose. (a-c) blue bubble is split in two, while in (d) blue bubble merges successively with yellow and green bubbles.

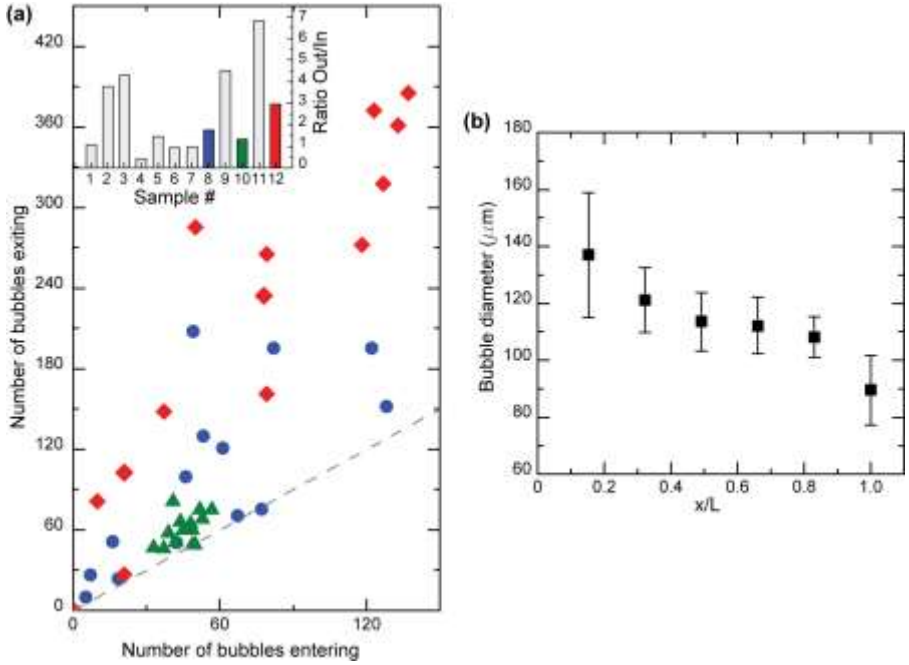

Fig. 7 Spatial characterization of bubble generation and destruction as the foam in the microporous environment. (a) Number of bubbles entering versus number of bubbles exiting the micromodel. Inset shows net bubble generation (out/in ratio) for multiple samples explored. (b) Average bubble sizes as a function of position in the micromodel.

mechanisms observed in CFs. Lamella division in CFs, as shown in **Fig. 6a**, occurs when a mobile bubble encounters a constriction that causes the flow to branch in two directions. The bubble stretches around the constriction, flows in both directions and divides into two separate bubbles that continue translating downstream.[37-38] In **Fig. 6b** we highlight the recently discovered pinch off mechanism that involves the interaction of two or more bubbles flowing through a constriction.[39] During pinch off, the bubble passing through a constriction is broken into separate pieces by a neighboring bubble attempting to pass through the same constriction. We also observe the more common snap off mechanism as shown in **Fig. 6c**. As described by Radke and Kovscek,[6] snap off is a mechanical process that repeatedly occurs in multiphase flow. Snap off occurs when a bubble enters a pore constriction and the liquid around the pore neck causes instability and leads to the "snap-off" of a new bubble.[40-41] Snap off is the dominant mechanism observed when gas and surfactant solution are co-injected to form high quality surfactant foams in porous media.[6, 42] In contrast, we observe that lamella division is the dominant bubble division mechanism in CFs flowing through the micromodel. Lastly, we note that the leave behind mechanism, where lenses are formed by the downstream convergence of bubbles that invade adjacent liquid filled pores, was not observed, likely because the degree of clogging in the pores and the low gas volume fraction in CFs preclude either gas flooding of adjacent pores and (or) downstream convergence of bubbles in the micromodel.[6, 43]

Lamella division depends on the bubble size and occupancy of the surrounding pores. We observe that bubble division typically occurs when the size of the approaching bubble exceeds the pore constriction size. However, we observed in a few cases that bubbles smaller than the constriction can also divide rather than flowing through one of the pores unaltered. Lamella division can also be prevented when bubbles or particles are trapped in neighboring pores. The stationary bubbles or particles prevent the bubble from dividing and force the approaching bubble to squeeze through the pore in one direction. Medium size bubbles can divide as many as 2-3 times before reaching the pore size and we observed that the number of divisions increases with bubble size.

In addition to the division and generation mechanisms highlighted, we observed that CF bubbles flowing through the micromodel also combine with one another in coalescence events and that large bubbles can flow through the pores unperturbed. As shown in **Fig. 6d**, coalescence of gas bubbles occurs when one bubble encounters another bubble flowing through the same channel or path. Coalescence in foams typically involves rupturing of thin films around bubbles. Large bubbles, that are created by coalescence or enter the micromodel as gas slugs, often span multiple pores and can translate through the micromodel without undergoing any division (see **Fig. 4c**). These gas slugs tend to invade multiple pores but only advance through one major channel. On exiting the micromodel, the branched gas fronts recede from the side paths and rejoin the flow through the primary path. To determine whether bubble generation or destruction dominates during flow through the micromodel, we estimated the net bubble generation rate by comparing the number of bubbles entering to the number of bubbles leaving the micromodel. **Fig. 7a** highlights the dispersity of the number of bubbles that entered the micromodel compared to the number of bubbles that left during a period of 0.25 s for three different

samples. The inset plot shows the net bubble generation ($R_{O/I}$: ratio of the number of bubbles exiting versus entering the micromodel) for all the samples explored; the ratio of colored samples corresponds to the samples in the main plot. The main plot in **Fig. 7a** shows that most of the scatter points are above the x = y line, indicating net positive bubble generation, *i.e.*, there are more generation than destruction events in general. The ratio in the inset plot measures the degree to which division and generation events dominate destruction events and further shows that, in some cases, the generation events can exceed destruction events by up to 7 times. We observed that the samples with higher net bubble generation ($R_{O/I} \geq 3$) correlate to flow of CF bubbles during a full or partial mobilization of the micromodel due to pressure bursts and that samples with $R_{O/I} \approx 1$ or slightly higher correlate to steady flow of CFs at relatively constant ΔP. The main plot in **Fig. 7a** shows that the ratio of bubbles entering and exiting the micromodel can vary significantly depending on the flow behavior observed. For steady flow (blue circles and green triangles), the scatter can be small or large with the bubble numbers varying based on the $R_{O/I}$ magnitude within the period. In contrast, for a full or partial mobilization (red diamonds), the scatter is very large with a higher bubble sample and $R_{O/I}$. In all cases sampled, $R_{O/I}$ rarely goes below 1 (see sample #4 in **Fig. 7a**) and the dominant process observed is bubble division.

To further characterize the effect of bubble division on CFs as they propagate through the porous medium, we investigated the changes in bubble sizes across the micromodel. The number of bubbles generally increases while the sizes of bubbles are observed to decrease with increasing position by length in the micromodel. **Fig. 7b** shows the plot of the average bubble sizes (in equivalent diameters of a sphere) measured as a function of position within the micromodel. The plot shows that the bubbles entering the micromodel are polydisperse with an average size that is ~1.4x larger than the constriction spacing in the micromodel ($100\ \mu m$). We also observed that the average size of CF bubbles prior to entering the micromodel increases between the beginning and end of stage II of CF flow. The average bubble diameter at the beginning of stage II was measured to be ~150 microns compared to ~170 microns toward the end of stage II. As the bubbles move through the first set of constrictions and pores, the average bubble size and its variability decrease. We observe in **Fig. 7b** that there are no significant changes to the bubble sizes and variations in the middle of the micromodel at positions $0.4 \leq x/l \leq 0.7$ and that the bubble sizes further decrease towards the exit/end of the micromodel. The average size of bubbles exiting the micromodel ($90\ \mu m$) is slightly lower than and comparable to the constriction length. The plot shows that the bubble size does not sharply decrease through the entire length of the micromodel as would be expected if bubble division alone occurred. The consistency in the average bubble sizes and variations, observed at the middle positions of the micromodel, results from a balance of bubble generation and destruction events where bubble sizes decrease because of bubble generation events and bubble sizes increase because of coalescence.

Overall, the porous environment favors bubble division which not only leads to more uniform bubble sizes but also contributes to the overall stability of capillary foams on a pore scale level. The higher bubbles count in conjunction with the particle network rigidity in CFs would favor pore blockage and fluid diversion across a microporous environment which in turn benefit sweep efficiency in fluid displacement operation like EOR.

4. Conclusions

We have investigated the flow behavior of capillary foams (CFs) at the pore length scale using a PDMS micromodel. CFs flow through porous environments and one can achieve recovery rates of ~90 % above a threshold flow rate. CF flow is not homogenous and three different regimes were identified through the micromodel: particle flow, bubble and particle co-flow, and flow of large gas slugs. The measured pressure drop required to mobilize the CF in these regimes increases with the gas volume fraction and depends on clogging within the micromodel. These phenomena directly lead to the absence of steady state foam flow. Moreover, analysis of bubble dynamics surprisingly shows that CFs share many bubble generation and destruction mechanisms with surfactant foams – lamella division, snap off, pinch off, and coalescence – and that bubble generation exceeds bubble loss during CF propagation in porous media. However, contrary to surfactant foams, the main mechanism of bubble generation is lamella division. The work in this study serves as a starting point to understand CF flow in porous media. The observed pore clogging, by bubbles and particles in CFs, may enable fluid diversion that improves sweep efficiency during oil displacement from underground pores. Combined with the inherent tunability of capillary foams and their stability under stress and in the presence of oil, our results on flow in porous media point to promise of capillary foams for oil recovery.

Author Contributions

Sven H. Behrens: 0000-0002-3528-4053
J. Carson Meredith: 0000-0003-2519-5003
Hang Lu: 0000-0002-6881-660X
Guillaume Aubry: 0000-0001-7828-8508
Omotola Okesanjo: 0000-0002-2123-6288

Conflicts of interest

There are no conflicts to declare.

Acknowledgements

The work in this paper was made possible with the financial support from the National Science Foundation (CBET-1706475). We would also like to acknowledge the generous donation of

silica particles from Wacker-Chemie AG (Germany). This work was performed in part at the Georgia Tech Institute for Electronics and Nanotechnology, a member of the National Nanotechnology Coordinated Infrastructure (NNCI), which is supported by the National Science Foundation (Grant ECCS-1542174).

References

1. Prud'homme, R. K.; Khan, S. A., *Foams: Theory: Measurements: Applications*. Taylor & Francis: New York, USA, 1995; Vol. 1, p 411-463.

2. Stevenson, P., *Foam Engineering: Fundamentals and Applications*. John Wiley & Sons: United Kingdom, 2012; Vol. 1, p 1-4.

3. Farajzadeh, R.; Andrianov, A.; Krastev, R.; Hirasaki, G. J.; Rossen, W. R., Foam-oil interaction in porous media: implications for foam assisted enhanced oil recovery. *Adv. Colloid Interface Sci.* **2012,** *183-184*, 1-13.

4. Ma, K.; Liontas, R.; Conn, C. A.; Hirasaki, G. J.; Biswal, S. L., Visualization of improved sweep with foam in heterogeneous porous media using microfluidics. *Soft Matter* **2012,** *8* (41).

5. Singh, R.; Mohanty, K. K., Foam flow in a layered, heterogeneous porous medium: A visualization study. *Fuel* **2017,** *197*, 58-69.

6. Kovscek, A. R.; Radke, C. J., Fundamentals of Foam Transport in Porous Media. In *Foams: Fundamentals and Applications in the Petroleum Industry*, 1994; pp 115-163.

7. Chen, M.; Yortsos, Y. C.; Rossen, W. R., Pore-network study of the mechanisms of foam generation in porous media. *Phys Rev E Stat Nonlin Soft Matter Phys* **2006,** *73* (3 Pt 2), 036304.

8. Zhang, Z. F.; Freedman, V. L.; Zhong, L., Foam Transport in Porous Media-A Review. Pacific Northwest National Laboratory, 2009; Vol. PNNL-18918.

9. Conn, C. A.; Ma, K.; Hirasaki, G. J.; Biswal, S. L., Visualizing oil displacement with foam in a microfluidic device with permeability contrast. *Lab Chip* **2014,** *14* (20), 3968-77.

10. Shojaei, M. J.; Osei-Bonsu, K.; Grassia, P.; Shokri, N., Foam Flow Investigation in 3D-Printed Porous Media: Fingering and Gravitational Effects. *Industrial & Engineering Chemistry Research* **2018,** *57* (21), 7275-7281.

11. Sun, Q.; Li, Z.; Wang, J.; Li, S.; Li, B.; Jiang, L.; Wang, H.; Lü, Q.; Zhang, C.; Liu, W., Aqueous foam stabilized by partially hydrophobic nanoparticles in the presence of surfactant. *Colloids and Surfaces A: Physicochemical and Engineering Aspects* **2015,** *471*, 54-64.

12. Fei, Y.; Johnson, R. L.; Gonzalez, M.; Haghighi, M.; Pokalai, K., Experimental and numerical investigation into nano-stabilized foams in low permeability reservoir hydraulic fracturing applications. *Fuel* **2018,** *213*, 133-143.

13. Yekeen, N.; Manan, M. A.; Idris, A. K.; Padmanabhan, E.; Junin, R.; Samin, A. M.; Gbadamosi, A. O.; Oguamah, I., A comprehensive review of experimental studies of nanoparticles-stabilized foam for enhanced oil recovery. *Journal of Petroleum Science and Engineering* **2018,** *164*, 43-74.

14. Sun, L.; Bai, B.; Wei, B.; Pu, W.; Wei, P.; Li, D.; Zhang, C., Recent advances of surfactant-stabilized N2/CO2 foams in enhanced oil recovery. *Fuel* **2019,** *241*, 83-93.

15. Zhang, Y.; Wu, J.; Wang, H.; Meredith, J. C.; Behrens, S. H., Stabilization of liquid foams through the synergistic action of particles and an immiscible liquid. *Angew. Chem. Int. Ed. Engl.* **2014,** *53* (49), 13385-9.

16. Okesanjo, O.; Meredith, J. C.; Behrens, S. H., Effect of Shear on Pumped Capillary Foams. *Industrial & Engineering Chemistry Research* **2023,** *62* (18), 7031-7039.

17. Behrens, S. H., Oil-coated bubbles in particle suspensions, capillary foams, and related opportunities in colloidal multiphase systems. *Current Opinion in Colloid & Interface Science* **2020,** *50*.

18. Okesanjo, O.; Meredith, J. C.; Behrens, S. H., Structure-Property Relationship in Capillary Foams. *Langmuir* **2021,** *37* (35), 10510-10520.

19. Okesanjo, O.; Tennenbaum, M.; Fernandez-Nieves, A.; Meredith, J. C.; Behrens, S. H., Rheology of capillary foams. *Soft Matter* **2020,** *16* (29), 6725-6732.

20. Wang, S. Oil-coated bubbles in complex colloidal systems: Fundamentals and applications. Doctoral Thesis, Georgia Institute of Technology, 2018.

21. Zhang, Y.; Allen, M. C.; Zhao, R.; Deheyn, D. D.; Behrens, S. H.; Meredith, J. C., Capillary foams: stabilization and functionalization of porous liquids and solids. *Langmuir* **2015,** *31* (9), 2669-76.

22. Zhang, Y.; Wang, S.; Zhou, J.; Benz, G.; Tcheimou, S.; Zhao, R.; Behrens, S. H.; Meredith, J. C., Capillary Foams: Formation Stages and Effects of System Parameters. *Industrial & Engineering Chemistry Research* **2017,** *56* (34), 9533-9540.

23. Xiao, S.; Zeng, Y.; Vavra, E. D.; He, P.; Puerto, M.; Hirasaki, G. J.; Biswal, S. L., Destabilization, Propagation, and Generation of Surfactant-Stabilized Foam during Crude Oil Displacement in Heterogeneous Model Porous Media. *Langmuir* **2018,** *34* (3), 739-749.

24. Osei-Bonsu, K.; Grassia, P.; Shokri, N., Investigation of foam flow in a 3D printed porous medium in the presence of oil. *J. Colloid Interface Sci.* **2017,** *490*, 850-858.

25. Wang, S.; Chen, C.; Kadum, M. J.; Shiau, B.-J.; Harwell, J. H., Enhancing foam stability in porous media by applying nanoparticles. *J. Dispersion Sci. Technol.* **2017,** *39* (5), 734-743.

26. Telmadarreie, A.; Doda, A.; Trivedi, J. J.; Kuru, E.; Choi, P., CO2 microbubbles – A potential fluid for enhanced oil recovery: Bulk and porous media studies. *Journal of Petroleum Science and Engineering* **2016,** *138*, 160-173.

27. Koos, E.; Willenbacher, N., Capillary Forces in Suspension Rheology. *Science* **2011,** *331* (6019), 897.

28. Duffy, D. C.; McDonald, J. C.; Schueller, O. J. A.; Whitesides, G. M., Rapid Prototyping of Microfluidic Systems in Poly(dimethylsiloxane). *Anal. Chem.* **1998,** *70* (23), 4974-4984.

29. Okesanjo, O.; Meredith, J. C.; Behrens, S. H., Dynamics and Aging in Capillary Foams. *In Review* **2022**.

30. Kozeny, J., Uber kapillare leitung der wasser in boden. *Royal Academy of Science, Vienna, Proc. Class I* **1927,** *136*, 271-306.

31. Carman, P. C., Fluid flow through granular beds. *Trans. Inst. Chem. Eng.* **1937,** *15*, 150-166.

32. Ozgumus, T.; Mobedi, M.; Ozkol, U., Determination of Kozeny Constant Based on Porosity and Pore to Throat Size Ratio in Porous Medium with Rectangular Rods. *Engineering Applications of Computational Fluid Mechanics* **2014,** *8* (2), 308-318.

33. Hemeida, A. M., Rheological Behavior of Saudi Crude Oils. *Journal of King Saud University - Engineering Sciences* **1990,** *2* (1), 181-193.

34. Saeed, S.; Aboul Fotouh, T. M.; Ashour, I., A Current Viscosity of Different Egyptian Crude Oils: Measurements and Modeling Over a Certain Range of Temperature and Pressure. *Journal of Petroleum & Environmental Biotechnology* **2016,** *07* (06).

35. Alomair, O.; Jumaa, M.; Alkoriem, A.; Hamed, M., Heavy oil viscosity and density prediction at normal and elevated temperatures. *Journal of Petroleum Exploration and Production Technology* **2016,** *6* (2), 253-263.

36. Firoze Akhtar, T.; Ahmed, R.; Elgaddafi, R.; Shah, S.; Amani, M., Rheological behavior of aqueous foams at high pressure. *Journal of Petroleum Science and Engineering* **2018,** *162*, 214-224.
37. Kam, S. I.; Rossen, W. R., A model for foam generation in homogeneous media. *Spe Journal* **2003,** *8* (4), 417-425.
38. Dicksen, T.; Hirasaki, G. J.; Miller, C. A., Conditions for Foam Generation in Homogeneous Porous Media. In *SPE/DOE Improved Oil Recovery Symposium*, Society of Petroleum Engineers: Tulsa, Oklahoma, 2002.
39. Liontas, R.; Ma, K.; Hirasaki, G. J.; Biswal, S. L., Neighbor-induced bubble pinch-off: novel mechanisms of in situ foam generation in microfluidic channels. *Soft Matter* **2013,** *9* (46).
40. Kovscek, A. R.; Radke, C. J., Gas bubble snap-off under pressure-driven flow in constricted noncircular capillaries. *Colloids and Surfaces a-Physicochemical and Engineering Aspects* **1996,** *117* (1-2), 55-76.
41. Kovscek, A. R.; Tang, G. Q.; Radke, C. J., Verification of Roof snap off as a foam-generation mechanism in porous media at steady state. *Colloids and Surfaces a-Physicochemical and Engineering Aspects* **2007,** *302* (1-3), 251-260.
42. Owete, O. S.; Brigham, W. E., Flow Behavior of Foam: A Porous Micromodel Study. *SPE Reservoir Engineering* **1987,** *2* (03), 315-323.
43. Almajid, M. M.; Kovscek, A. R., Pore-level mechanics of foam generation and coalescence in the presence of oil. *Adv. Colloid Interface Sci.* **2016,** *233*, 65-82.